Physica C 508 (2015) 31–35

Contents lists available at ScienceDirect

Physica C

journal homepage: www.elsevier.com/locate/physc

A revision of the fishtail effect in $YBa_2Cu_3O_{7-\delta}$ crystals and its connection with vortex dynamics

D. Pérez Daroca [b], G. Pasquini [a,*]

[a] Departamento de Física, FCEyN, Universidad de Buenos Aires and IFIBA, CONICET, Pabellon 1, Ciudad Universitaria, 1428 Buenos Aires, Argentina
[b] Gerencia de Investigación y Aplicaciones, Comisión Nacional de Energía Atómica and CONICET, Av. General Paz 1499, 1650 San Martín, Buenos Aires, Argentina

ARTICLE INFO

Article history:
Received 20 September 2014
Received in revised form 20 October 2014
Accepted 29 October 2014
Available online 8 November 2014

Keywords:
74.25.Uv YBCO
Fishtail magnetization
Peak Effect
History effects
Vortex creep regimes

ABSTRACT

The fishtail magnetization observed in many type II superconductors has been investigated since the earliest nineties and associated with different phase transitions and dynamic crossovers in complex vortex matter. In systems without a sharp order–disorder phase transition, the fishtail has been related with a crossover from elastic to plastic vortex creep regimes. In this paper we perform a critical revision of this accepted picture. We show that, in slightly underdoped $YBa_2Cu_3O_{7-\delta}$ single crystals, there is a clear correlation between the fishtail magnetization and the Peak Effect observed in *ac* experiments with the associated history effects. We propose that both features are originated in the same dynamic crossover, between two plastic creep regimes. The proposed picture can also apply to other system, as those belonging to same families of iron-based pnictides.

1. Introduction

In the vortex lattice (VL) of type II superconductors elastic and pinning interactions together with thermal fluctuations compete, giving rise to complex behaviors [1]. One of the consequences of this complexity is the well known fishtail magnetization [2], a non-monotonous dependence of the irreversible magnetization M_{irr} with the applied magnetic field H, whose physical origin has been investigated from the earliest nineties and associated with different phase transitions and dynamic crossovers.

In this context, the extensively studied cuprate $YBa_2Cu_3O_{7-\delta}$ (YBCO) is particularly interesting. In these samples, the phase diagram as well as the fishtail physical origin, are strongly modified by subtle changes in the oxygen doping level δ. In optimally doped and slightly overdoped crystals, a minimum in the irreversible magnetization curve as a function of the applied field $M_{irr}(H)$ at $H = H_{on}$, followed by a maximum in a upper field $H = H_p$ are observed and indicate a non-monotonic dependence of the measured critical current density J_c. In those samples, the maximum in the measured J_c at H_p indicates an order–disorder (O–D) transition from an ordered Bragg Glass (BG) to a disordered Vortex Glass (VG) at higher fields and/or temperatures [3,4]; H_p increases with temperature (T) and disappears after crossing the melting line at the critical point [5]. On the other hand, in slightly underdoped crystals, there is no trace of the melting transition. There is also a minimum in $M_{irr}(H_{on})$ and a maximum in $M_{irr}(H_p)$ but, in those cases, H_p decreases with T up to crossing the irreversibility line $H_{irr}(T)$ and depends on the acquisition time [3,6]. These facts, including non monotonous current relaxation rate S, indicate that, in slightly underdoped YBCO crystals, the fishtail magnetization is related with a dynamic crossover. The nature of this crossover has been investigated by several groups in the nineties [6,7]. Whereas in the first studies the maximum in the critical current at H_p had been attributed to a dimensional pinning crossover [7], some years later a crossover from an elastic to a plastic creep regime has been proposed as the origin of the fishtail magnetization [6]. This second picture assumes a finite plastic creep activation barrier U_{pl}^0 at $J = 0$ (in agreement with the theories developed at that time) to explain the increase in the creep rate and the decrease in the measured J_c with increasing field observed above H_p, in the plastic creep regime. However, different experiments showed that the disordered phase has an apparent higher J_c [8]. In the following decade, the role of the dislocations in the vortex dynamics has been extensively studied and both experimental and theoretical works demonstrated that divergent plastic barriers at small driving currents are expected in the plastic vortex creep, with higher critical exponents that those expected from the elastic creep [9,10]. However, the original fishtail description has been maintained, and further extended for various authors (including

* Corresponding author at: Departamento de Física, FCEyN, Universidad de Buenos Aires and IFIBA, CONICET, Pabellon 1, Ciudad Universitaria, 1428 Buenos Aires, Argentina.
E-mail address: pasquini@df.uba.ar (G. Pasquini).

http://dx.doi.org/10.1016/j.physc.2014.10.017
0921-4534/

some of us) [11,12] to describe the phase diagram of other compounds displaying a similar phenomenology, as some families of pnictides superconductors.

At the present time there is consensus that the proliferation of dislocations increases the apparent critical current density J_c and reduces the VL mobility. The VL disordering causes the well known Peak Effect (PE) [13] anomaly, observed in both *ac* susceptibility and transport experiments. In all the cases, metastability and VL history effects are concurrently observed in the PE region [14–17], and associated with history dependent VL configurations with different dislocation densities. Whereas in the presence of a first order O–D transition there is a sharp PE, in the slightly underdoped YBCO crystals, at intermediate magnetic fields, a broad dynamic PE can be observed [15–17], and very particular dynamic history effects occurs: the VL mobility increases after applying a high *dc* transport current and can be increased or even decreased by applying different shaking *ac* fields, being the proposed scenario a dynamic reordering of the VL [15].

Based in the previous considerations, in this paper we perform a critical revision of the accepted picture that explains the fishtail magnetization in slightly underdoped YBCO and other compounds based in a crossover from an elastic to a plastic regime. We show that, in slightly underdoped YBCO single crystals, there is a clear correlation between the fishtail magnetization, the PE observed in *ac* experiments, and the associated history effects. We propose that both features are originated for the same dynamic crossover, and we discuss the underlying physics.

2. Experimental

Experiments were carried out in $YBa_2Cu_3O_{7-\delta}$ single crystals [18]. Results shown in this work correspond to a single crystal of approximated dimensions $(0.55 \times 0.45 \times 0.05)$ mm^3, with $T_c = 92.5$ K (defined as the onset of the *ac* shielding at $H = 0$) and a transition width (defined between 5% and 95% of the complete shielding in the linear regime) $\Delta T_c \sim 0.3$ K. Light polarized images show domains of twin boundaries, so experiments were performed with the applied *dc* magnetic field rotated in an angle $\theta \sim 20^\circ$ relative to the crystal *c* axis in a plane rotated approx 45° from both twin plane orientations, in order to avoid the Bose Glass phase. Magnetization and *ac* susceptibility measurements at $f = 1$ kHz were carried out in a Quantum Design MPMS 7 Tesla SQUID magnetometer equipped with Reciprocating Sample Option (RSO) and *ac* accessories. In this setup, the *ac* and *dc* field are both in the same direction. In all the susceptibility measurements, the in-phase and out of phase components of the first harmonic *ac* susceptibility (χ' and χ'') were normalized in way that $\chi' = \chi'' = 0$ when the *ac* field fully penetrate the sample (normal state) and $\chi' = -1$, $\chi'' = 0$ when the *ac* field is completely screened (superconducting state with $H = 0$). To obtain the magnetization of the samples, magnetic moment has been recorded with an RSO accessory using 1 Hz, ±1 cm excursions from the center of the coils. The diamagnetic background coming from the sample holder has been subtracted. Because the center of the sample holder and sample are not identical, the quantitative fit of the sample magnetic moment at high temperatures (when both magnetic moments are comparable) is not accurate, but can be used for the qualitative approach of this paper.

3. Results and discussion

Example of irreversible magnetization curves as a function of the applied magnetic field $\mu_0 H$ for various temperatures are shown in Fig. 1 in logarithmic scale. The reversible magnetization is only significant at the higher temperatures, when the measured critical current drops. An example of a full $M(H)$ curve at high temperature is shown in the inset, with the reversible diamagnetic field expulsion is indicated in dashed line. In the main panel, the characteristic fields H_{on} (green squares), H_p (blue squares) and H_{irr} (red squares) are indicated in each curve. Around H_{on} (local minimum in $M_{irr}(H)$) there is a region where M_{irr} is nearly H independent, signaled with horizontal error bars in the figure. H_p indicate the local maximum in $M(H)$, and H_{irr} the fields where $M_{irr} \sim 0$ at each T within our experimental resolution. We are able to measure an irreversible *dc* magnetization up to $T = 90.5$ K. The fishtail is observed up to this temperature, and all the characteristic fields decreases with increasing T. These features, together with the nearly optimal T_c approx 92.5 K, are in agreement with that expected for slightly underdoped samples [3].

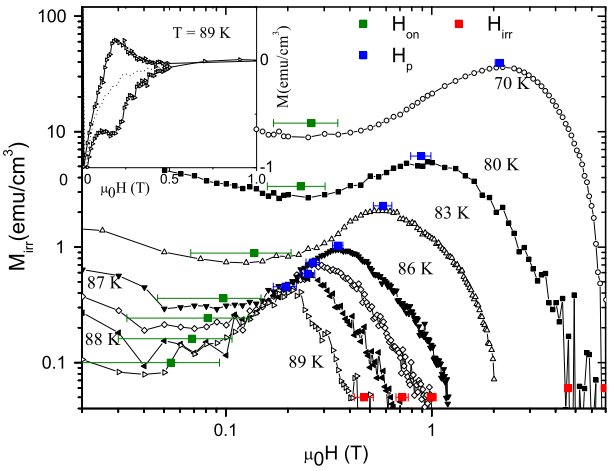

Fig. 1. (Main panel) Irreversible magnetization curves as function of the applied field $\mu_0 H$ for various temperatures plotted in logarithmic scale. Green, red and blue squares indicate the characteristic fields H_{on}, H_p and H_{irr} (see text). (Inset) Full $M(H)$ curve at $T = 89$ K, reversible diamagnetic field expulsion is indicated in dashed line. (For interpretation of the references to colour in this figure legend, the reader is referred to the web version of this article.)

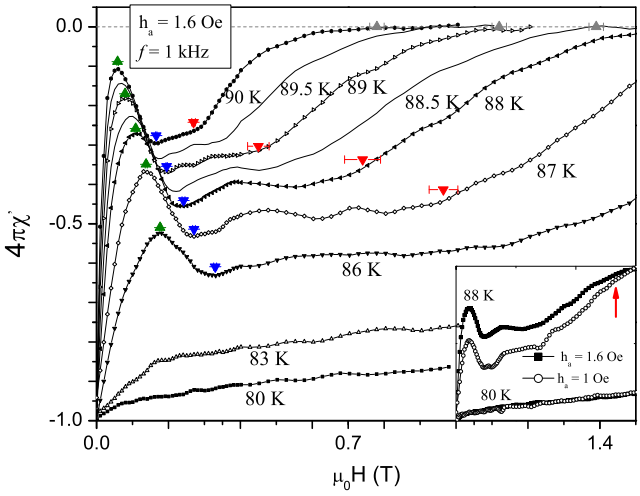

Fig. 2. (Main panel) In-phase component of the *ac* susceptibility as a function of the applied *dc* field $4\pi\chi'(H)$, measured at $f = 1$ kHz with an *ac* amplitude $h_a = 1.6$ Oe, at various temperatures. Green, blue, red and gray triangles indicate the characteristic fields H_1, H_2, H_3 and H_4 (see text). (Inset) Normalized responses obtained at two different *ac* amplitudes at two selected temperatures. The vertical arrow indicates the crossover to the linear Ohmic response. (For interpretation of the references to colour in this figure legend, the reader is referred to the web version of this article.)

Fig. 2 shows examples of the in-phase component of the *ac* susceptibility as a function of the applied *dc* field $4\pi\chi'(H)$, measured at $f = 1$ kHz with an *ac* amplitude $h_a = 1.6$ Oe, at various temperatures. At high T, pinning is weak, and the small *ac* field is enough to move vortices in the bulk sample; in this situation, the non-linear *ac* response displays a sharp peak at low fields, indicating a strong suppression in the vortex mobility between a local maximum in χ' at H_1 (green triangles) and a local minimum at H_2 (blue triangles), followed by a region where $\frac{\partial\chi}{\partial H}$ is smaller and χ' is nearly H independent. In the inset, the normalized responses obtained at two different *ac* amplitudes at two selected temperatures are shown; whereas at high T (where the peak is observed) the response is non-linear (i.e. amplitude dependent), below $T \sim 80$ K a linear response (i.e. amplitude independent) is obtained. This is not surprising: at low T, pinning is stronger and therefore the *ac* field only penetrates the outer region of the sample, moving the pinned vortices inside their pinning potential well, in a Campbell regime [19]. As shown in Ref. [20], the dynamic PE is not present in the Campbell regime. Above H_3 (red triangles) the mobility increases faster with H due to the VL depinning preceding the linear Ohmic response (arrow in the inset), before the complete *ac* sample penetration, at $H \sim H_4$ (gray triangles).

To compare magnetization results with *ac* susceptibility measurements, a brief review of their connection with vortex dynamic could be useful:

As it is well known, if a superconducting sample in the critical state is fully penetrated by the magnetic field B, the irreversible magnetization M_{irr} is proportional to J_c. In high-Tc superconductors, due to the high thermal activated motion, the current density flowing in the sample can be much lower than the "true" critical current density J_{c0}. However, as long as a strong non-linear current–voltage law $E(J)$ persists, the problem can be approximated by a critical state response, with a time dependent effective critical current density $J_c \propto M_{irr}$, being the proportion a geometrical factor [1].

On the other hand, when a small *ac* magnetic field $h_{ac}(t) = h_a \cos\omega t$ is added to a much larger *dc* field H, different regimes can hold. At low T and H, in the region of very strong pinning, the *ac* field is shielded and only the outer vortices move, inside their pinning potential well, in a linear Campbell regime. If the *ac* amplitude is small enough, the linear response can extend up to the liquid phase. However, at typical *ac* amplitudes (~ 1 Oe), at high T, vortex displacement are larger, so vortices move across various pinning centers and the *ac* penetration depth Λ_{ac} can be associated with the vortex mobility. If the strong non-linear law $E(J)$ persists, an effective frequency dependent $J_c(\omega) \propto h_a/\Lambda_{ac}$ holds, being the proportion a geometrical factor [1]. The function $\chi'(\Lambda_{ac})$ depends on the dynamic regime and geometry but, in the case of a non-linear response $E(J) = E_c(J/J_c)^n$, there is a weak dependence with the particular geometry and the creep exponent n [21]. Therefore, an approximate estimation of the effective Λ_{ac} can be obtained by inverting the function $\chi'(\Lambda_{ac})$ [21] for a thin disk in a Bean critical state ($n \to \infty$) proposed by Clem [22]. Without aim to quantitatively calculate the critical density current, we can qualitatively compare the effective J_c obtained from *ac* and *dc* measurements in the higher $T > 83$ K region.

In Fig. 3, $J_c(\omega) \propto 1/\Lambda_{ac}(\chi')$ (panel a) and $J_c \propto M_{irr}$ (panel b) measured at various T are plotted in arbitrary units, and can be compared up to a geometrical multiplicative factor. Vertical lines identify the characteristic fields H_1 (blue), H_2 (green) and H_3 (red) identified in Fig. 2. There is a clear correlation between the minimum and the maximum in J_c at each T revealing that the non-monotonous $\chi'(H)$ and the fishtail in $M(H)$ have the same origin. However, whereas above H_p (maximum in J_c identified in Fig. 2) the J_c estimated from *dc* measurements strongly drops,

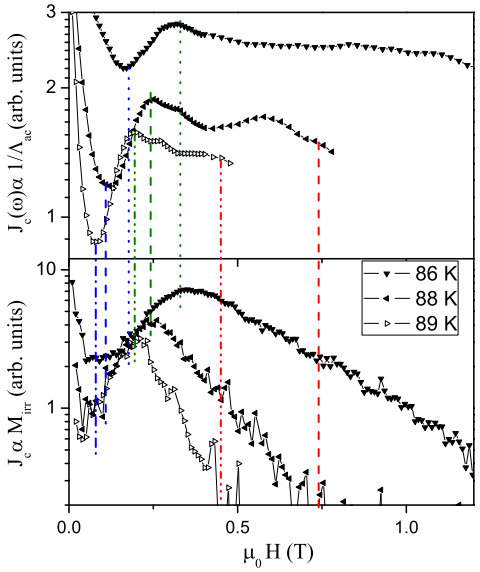

Fig. 3. $J_c(\omega) \propto 1/\Lambda_{ac}(\chi')$ (panel a) and $J_c \propto M_{irr}$ (panel b) measured at various T in arbitrary units. Vertical lines identify the characteristic fields H_1 (blue), H_2 (green) and H_3 (red) named in Fig. 2. There is a clear correlation between the minimum and the maximum in J_c at each T. (For interpretation of the references to colour in this figure legend, the reader is referred to the web version of this article.)

the *ac* penetration depth slowly decreases up to the upper field H_3, that precedes the irreversibility line. This fact is consistent with previous results, that report an increasing creep rate with increasing magnetic fields above H_p [6]. The correlation can be better appreciated in the dynamic phase diagram built in Fig. 4: the characteristic fields obtained in the high T region by *ac* measurements H_1 (green) H_2 (blue) and H_3(red) (see Fig. 2) and the onset of the *ac* diamagnetic signal (gray) are plotted with full triangles, together with the characteristic fields obtained from *dc* measurements H_{on} (green), H_p (blue) and H_{irr} (red) (see Fig. 1) plotted with full squares. The onset of the *ac* shielding (gray symbols) corresponds to the points where the flux flow resistivity is high enough to fully penetrate the sample (around 1 μΩ cm) at each H. The dashed line indicates the estimated $H_{c2}(T) \approx 1.6\ T/\mathrm{K}(T - T_c)$. Below this line, in the superconducting phase, four regions can be identified: Region

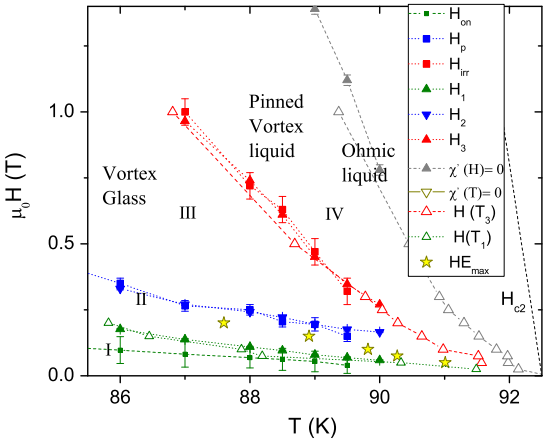

Fig. 4. Dynamics phase diagram, *dc* field, $\mu_0 H$ as a function of temperature. Full squares (triangles) are characteristic H identified in $M(H)(X(H))$ curves (Figs. 1 and 2); hollow triangles are characteristic T identified in $X'(T)$ curves (Fig. 5). Four regions are identified: vortex liquid (IV) and three dynamics region inside the vortex glass phase (I, II, III, see text). Dynamics and history effects (HE, yellow stars) are observable in Region III and II. (For interpretation of the references to colour in this figure legend, the reader is referred to the web version of this article.)

IV corresponds to the vortex liquid. Above the (resolution dependent) irreversibility line, there is a pinned liquid (called amorphous phase in some references [23]), followed by an ohmic liquid before H_4. In the vortex glass phase, three dynamic regions are identified as Region I (below H_1), Region II ($H_1 < H < H_2 \sim H_p$), and Region III, above the maximum in J_c. The key point that we would like to focus in the following is the relationship between these regions and the existence of dynamic and thermal history effects.

In the above experiments, the magnetic field was swept at fixed T, so the vortex entry and exit difficult the observation of dynamic history effects, frequently reported in *ac* susceptibility field-cooled experiments, performed at fixed H. Moreover, in the MPMS setup, even at fixed applied H, the sample moves through field gradients larger than the *ac* field, and the induced currents move vortices, avoiding a good control of the dynamic history. However, in slightly underdoped YBCO crystals, thermal history effects can be observed in non-linear $\chi'(T)$ curves as well as in resistance $R(T)$ curves [24]. In both cases, there is a higher VL mobility in the warming processes, that could be associated with a VL ordering at low T. Fig. 5 shows examples of field-cooled $\chi'(T)$ curves at different H recorded in cooling (FCC) and warming (FCW) T procedures. Thermal history effects are present at intermediate fields (in this sample 200 Oe $\lesssim H \lesssim$ 3000 Oe), in the T region below the temperature $T_3(H)$ (indicated with red hollow up triangles in Fig. 5) where $\frac{\partial \chi}{\partial T}$ suddenly increases toward a vanishing diamagnetic shielding near T_4 (gray hollow down triangles in Fig. 5). Below T_3, $\frac{\partial \chi}{\partial T}$ decreases. At intermediate fields, there is a region where χ' is nearly T independent and thermal history effects are maxima, vanishing around the lower temperature $T_1(H)$ (green hollow up triangles in Fig. 5). In experiments performed in a homemade susceptometer (where the sample is attached to a fixed position) it can be seen that dynamic history effects extend to lower temperatures and higher fields, in all the region below T_3 [15]. These characteristic temperatures at various *dc* fields are also included in the dynamic phase diagram with hollow triangles. The line $T_3(H)$ (red), as expected, coincides with the line $H_3(T)$, where the *ac* penetration depth suddenly increases due to the vanishing pinning near the irreversibility line $H_{irr}(T)$. On the other hand, the line $T_1(H)$ (green), that indicates the lower T limit where thermal history effects are observable, coincides with $H_1(T)$ and the lower limit of Region II. We define the maximum history effect at each H (yellow stars in Fig. 4) as the T where $\chi'_{FCW} - \chi'_{FCC}$ (see Fig. 5) is maximum.

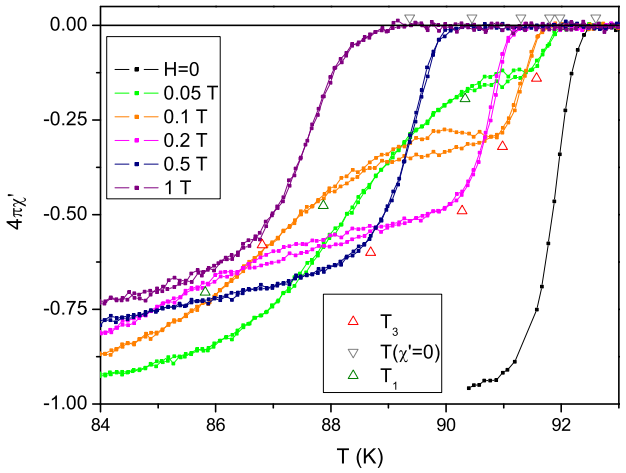

Fig. 5. Field-cooled $\chi'(T)$ curves at different H recorded in cooling and warming T procedures. Red hollow up triangles, $T_3(H)$, indicate where $\frac{\partial \chi}{\partial T}$ suddenly increases toward a vanishing diamagnetic shielding (gray hollow down triangles, $T(\chi' = 0)$). Green hollow up triangles, $T_1(H)$, indicate the temperature where thermal history effects vanish. (For interpretation of the references to colour in this figure legend, the reader is referred to the web version of this article.)

We arrive now to the goal that we want to emphasize in the present work: history effects in the *ac* response are observable in both Regions III and II. These effects are lager in Region II at $H < H_p$. There is a consensus in the community that these effects are due to the creation and/or annihilation of dislocations strongly associated to plastic dynamics and plastic creep. In fact, plastic dynamics below and above the minimum in $\chi'(H_2)$ is not surprising, and was already pointed out in 1998 by Aouaroun and Simon [25], from results in BSCCO samples. Therefore, the interpretation of the fishtail effect as a crossover from an elastic (dislocation free) to a plastic creep regime is not consistent with the observed correlation between H_2 and H_p.

The theory of plastic vortex creep [10], describes the thermally activated dynamics of a medium with a vortex dislocations density n_D, in a medium with a weakly first order BG–VG transition, occurring when the mean distance between dislocations $(n_D)^{-1/2}$ decreases below the positional correlation length R_a, on which typical elastic vortex displacement are of the order of the lattice constant a. Although in slightly underdoped YBCO crystals there is no evidence of this transition, some results regarding the vortex dislocation dynamics would be of help. Authors [10] demonstrated that plastic creep exponents characteristic of single dislocation creep regimes are much higher that those expected from elastic creep, so the thermally activated current decay is drastically reduced, producing an apparent increase in the measured J_c. However, with increasing magnetic field a critical point is reached when $(n_D)^{-1/2} \sim a$, beyond which the dislocation bundles creep dominates with much lower creep exponent. The system is an amorphous pinned solid, with the same spatial symmetry that the vortex liquid phase up to the field where thermal fluctuations dominate and pinning vanishes.

We propose that, in these samples, the fishtail effect could be related with a dynamic crossover from a regime of single dislocation creep to one of dislocation bundles. Above H_1 (Region II in Fig. 4) dislocation density increases, reducing the vortex mobility (and therefore the *ac* penetration depth) and increasing the measured J_c (Fig. 3). In this region, the dislocation density depends on the history and influences the vortex mobility (history effects in the *ac* response). Above H_p (Region III in Fig. 4) there is a drastic decay of the measured J_c, but the mobility is still reduced due to the high dislocation density, up to the liquid phase. This picture is also consistent with the (time dependent) increase of creep rate observed above H_p in other works [6].

4. Conclusions

By means of magnetization and *ac* susceptibility measurements in slightly underdoped YBCO, we have carried out a critical revision of the accepted fishtail magnetization picture. We have shown that there is a clear correlation between the fishtail magnetization, the PE observed in *ac* susceptibility measurements and the associated history effects, indicating that plastic dynamic dominates in both sides of the magnetization peak. We propose that, in these samples, the fishtail effect could be related with a dynamics crossover from a regime of single dislocation creep to one of dislocation bundles. This picture could also apply to other systems, as those belonging to the $Ba(Fe_xCo_{1-x})_2As_2$ iron-based pnictides where the absence of an ordered phase [26], together with the dynamic characteristics of the fishtail effect [11], are consistent with the proposed scenario.

Acknowledgment

We thank V. Bekeris for useful discussions. This work was partially supported by CONICET, ANPCyT, UBACyT.

References

[1] G.W. Crabtree, D.R. Nelson, Phys. Today 50 (1986) 38;
G. Blatter, M.V. Feigelman, V.B. Geshkenbein, A.I. Larkin, V.M. Vinokur, Rev. Mod. Phys. 66 (1994) 1125.
[2] M. Däumling, J.M. Seuntjens, D.C. Larbalestier, Nature 346 (1990) 332.
[3] K. Shibata, T. Nishizaki, T. Sasaki, N. Kobayashi, Phys. Rev. B 66 (2002) 214518.
[4] T. Nishizaki, T. Naito, N. Kobayashi, Phys. Rev. B 58 (1998) 11169;
S. Kokkaliaris, P.A.J. de Groot, S.N. Gordeev, A.A. Zhukov, R. Gagnon, L. Taillefer, Phys. Rev. Lett. 82 (1999) 5116.
[5] K. Deligiannis, P.A.J. de Groot, M. Oussena, S. Pinfold, R. Langan, R. Gagnon, L. Taillefer, Phys. Rev. Lett. 79 (1997) 2121.
[6] Y. Abulafia, A. Shaulov, Y. Wolfus, R. Prozorov, L. Burlachkov, Y. Yeshurun, D. Majer, E. Zeldov, H. Wuhl, V.B. Geshkenbein, V.M. Vinokur, Phys. Rev. Lett. 77 (1996) 1596.
[7] L. Krusin-Elbaum, L. Civale, V.M. Vinokur, F. Holtzberg, Phys. Rev. Lett. 69 (1992) 2280.
[8] A few examples in different materials: B. Khaykovich et al., Phys. Rev. Lett. 76 (1996) 2555;
M. Menghini, Yanina Fasano, F. de la Cruz, Phys. Rev. B 65 (2002) 064510.
[9] C.J. van der Beek, S. Colson, M.V. Indenbom, M. Konczykowski, Phys. Rev. Lett. 84 (2000) 4196.
[10] J. Kierfeld, H. Nordborg, V.M. Vinokur, Phys. Rev. Lett. 85 (2000) 4948.
[11] R. Prozorov, N. Ni, M.A. Tanatar, V.G. Kogan, R.T. Gordon, C. Martin, E.C. Blomberg, P. Prommapan, J.Q. Yan, S.L. Budko, P.C. Canfield, Phys. Rev. B 78 (2008) 224506;
B. Shen, P. Cheng, Z. Wang, L. Fang, C. Ren, L. Shan, H.-H. Wen, Phys Rev. B 81 (2010) 014503.
[12] M. Marziali Bermudez, G. Pasquini, S.L. Budko, P.C. Canfield, Phys. Rev. B 87 (2013) 054515.
[13] A.B. Pippard, Proc. R. Soc. London A 216 (1953) 547.
[14] See, for example: W. Henderson, E.Y. Andrei, M.J. Higgins, Phys. Rev. Lett. 81 (1998) 2352;
Z.L. Xiao, E.Y. Andrei, M.J. Higgins, ibid. 83 (1999) 1664;
G. Pasquini, D. Perez Daroca, C. Chiliotte, G. Lozano, V. Bekeris, Phys. Rev. Lett. 100 (2008) 247003.
[15] S.O. Valenzuela, V. Bekeris, Phys. Rev. Lett. 86 (2001) 504;
G. Pasquini, D. Luna, G. Nieva, Phys. Rev. B 76 (2007) 212302.
[16] D. Stamopoulos, M. Pissas, A. Bondarenko, Phys. Rev. B 66 (2002) 214521.
[17] G. Pasquini, V. Bekeris, Supercond. Sci. Techol. 19 (2006) 671.
[18] I.V. Aleksandrov, A.B. Bykov, I.P. Zibrov, I.N. Makarenko, O.K. Melnikov, V.N. Molchanov, L.A. Muradyan, D.V. Nikiforov, L.E. Svistov, V.I. Simonov, S.M. Chigishov, A.Y. Shapiro, S.M. Stishov, JETP Lett. 48 (1988) 493;
F. de la Cruz, D. Lopez, G. Nieva, Philos. Mag. B 70 (1994) 773.
[19] A.M. Campbell, J. Phys. C 2 (1969) 1492;
A.M. Campbell, ibid. 4 (1979) 3186.
[20] G. Pasquini, V. Bekeris, Phys.Rev. B 71 (2005) 014510.
[21] E.H. Brandt, Phys. Rev. B 55 (1997) 14513.
[22] J.R. Clem, A. Sanchez, Phys. Rev. B 50 (1994) 9355.
[23] D. Dal, S. Ramakrishnan, A.K. Grover, D. Dasgupta, Bimal K. Sarma, Supercond. Sci. Technol. 15 (2002) 258.
[24] S.O. Valenzuela, B. Maiorov, E. Osquiguil, V. Bekeris, Phys. Rev. B 65 (2002) 060504.
[25] T. Aouaroun, Ch. Simon, Phys. Rev. B 58 (1998) 11692.
[26] M.R. Eskildsen, L. Ya. Vinnikov, T.D. Blasius, I.S. Veshchunov, T.M. Artemova, J.M. Densmore, C.D. Dewhurst, N. Ni, A. Kreyssig, S.L. Budko, P.C. Canfield, A.I. Goldman, Phys. Rev.B 79 (2009) 100501.